Phase transformation behavior of a two-dimensional zeolite

Zeolites

International Edition: DOI: 10.1002/anie.201904825
German Edition: DOI: 10.1002/ange.201904825

Phase Transformation Behavior of a Two-Dimensional Zeolite

Juna Bae[+], Magdalena O. Cichocka[+], Yi Zhang, Zoltán Bacsik, Sara Bals, Xiaodong Zou, Tom Willhammar, and Suk Bong Hong**

Abstract: *Understanding the molecular-level mechanisms of phase transformation in solids is of fundamental interest for functional materials such as zeolites. Two-dimensional (2D) zeolites, when used as shape-selective catalysts, can offer improved access to the catalytically active sites and a shortened diffusion length in comparison with their 3D analogues. However, few materials are known to maintain both their intralayer microporosity and structure during calcination for organic structure-directing agent (SDA) removal. Herein we report that PST-9, a new 2D zeolite which has been synthesized via the multiple inorganic cation approach and fulfills the requirements for true layered zeolites, can be transformed into the small-pore zeolite EU-12 under its crystallization conditions through the single-layer folding process, but not through the traditional dissolution/recrystallization route. We also show that zeolite crystal growth pathway can differ according to the type of organic SDAs employed.*

Zeolites, an important class of industrial catalysts and separation media, are covalently bonded three-dimensional (3D) networks of tetrahedrally coordinated framework atoms (T-atoms) bridged by oxygen atoms,[1] and layered zeolites consist of 2D sheets with growth limited in the third direction where they are interconnected via hydrogen bonds.[2] Since the discovery of MCM-22(P), the layered precursor of zeolite MCM-22 (framework type MWW), the 2D to 3D transformation of layered zeolites by post-synthetic treatments, such as calcination has been regarded as one way of finding novel zeolite structures.[2,3] From a structural standpoint, however, the two great advantages of the use of 2D zeolites as catalysts are the high accessibility of large reactant molecules to the catalytic sites and the low diffusion limit of both reactant and product molecules. Such benefits can be realized when 2D zeolites have intralayer microporosity even after calcination to remove organic structure-directing agents (SDAs) used, or when the external surface of their crystallites have zeolitic character.

When the "ultrathin" zeolites synthesized using organic SDAs with long surfactant moieties, which sterically hinder the zeolite crystal growth along the third dimension, are excluded from the more than 15 layered zeolites prepared by direct synthesis so far,[2,4] there are only four known materials: MCM-22(P) with 2D sinusoidal 10-ring channels, MCM-56, which is a disordered collection of MCM-22(P) monolayers, CIT-10 with the *rth*-type layer structure and ITQ-8 with the *lev*-type layer structure.[3,5] Unfortunately, all of them, with the exception of MCM-56, topologically condense into 3D framework materials or structurally collapse upon calcination. Herein we report the synthesis and structure of a new layered zeolite, denoted PST-9, the intralayer microporosity of which is retained even after removal of the occluded organic SDA at 550 °C. We also demonstrate that PST-9 can undergo an in situ phase transformation to EU-12 (ETL), a channel-based, small-pore zeolite, in the crystallization medium. This transformation was characterized to proceed via a single-layer folding growth mechanism, which has been neither observed nor proposed in ordered nanoporous materials chemistry.

We first noticed PST-9 as an intermediate phase during EU-12 synthesis under rotation (60 rpm) at 150 °C using an aluminosilicate gel with the oxide composition $2.0\,ChCl{\cdot}0.7\,Rb_2O{\cdot}0.3\,Na_2O{\cdot}0.25\,Al_2O_3{\cdot}5.0\,SiO_2{\cdot}100\,H_2O$, where ChCl is choline ((2-hydroxyethyl)trimethylammonium) chloride.[6] We were able to obtain this material as its pure form after 2 days of heating, although its crystallization prefers the use of two different types of alkali metal cations in the presence of choline used as an organic SDA, that is, the so-called multiple inorganic cation approach.[6,7] Interestingly, the stability of PST-9 in the crystallization medium was found to differ notably according to the type of secondary alkali metal cations (Table S1 in the Supporting Information). Thus, to minimize impurity effects, the sample (ChRbLi-PST-9) obtained after 28 days of heating at 150 °C was used in the structural characterization of PST-9.

As-made ChRbLi-PST-9 crystallizes as warped thin sheets of approximately 1.5 nm in thickness (Figure S1), and no noticeable periodicity is observed along the direction perpendicular to the sheet itself (Figure 1 a,b). However, thermal analysis reveals an exothermic loss in weight of around 8 wt % around 620 °C even after repeated K^+ ion exchange, suggesting the constrained encapsulation of choline within the PST-9 pores (Figures S2 and S3). The ^{29}Si MAS NMR spectrum of

[*] J. Bae,[+] Prof. S. B. Hong
Center for Ordered Nanoporous Materials Synthesis
Division of Environmental Science and Engineering, POSTECH
Pohang 37673 (Korea)
E-mail: sbhong@postech.ac.kr
Dr. M. O. Cichocka,[+] Y. Zhang, Z. Bacsik, Prof. X. Zou, Prof. T. Willhammar
Berzelii Center EXSELENT on Porous Materials
Department of Materials and Environmental Chemistry
Stockholm University
106 91 Stockholm (Sweden)
E-mail: tom.willhammar@mmk.su.se
Prof. S. Bals
Electron Microscopy for Materials Science (EMAT)
University of Antwerp
Groenenborgerlaan 171, 2020 Antwerp (Belgium)
[+] These authors contributed equally to this work.
Supporting information and the ORCID identification number(s) for the author(s) of this article can be found under: https://doi.org/10.1002/anie.201904825.

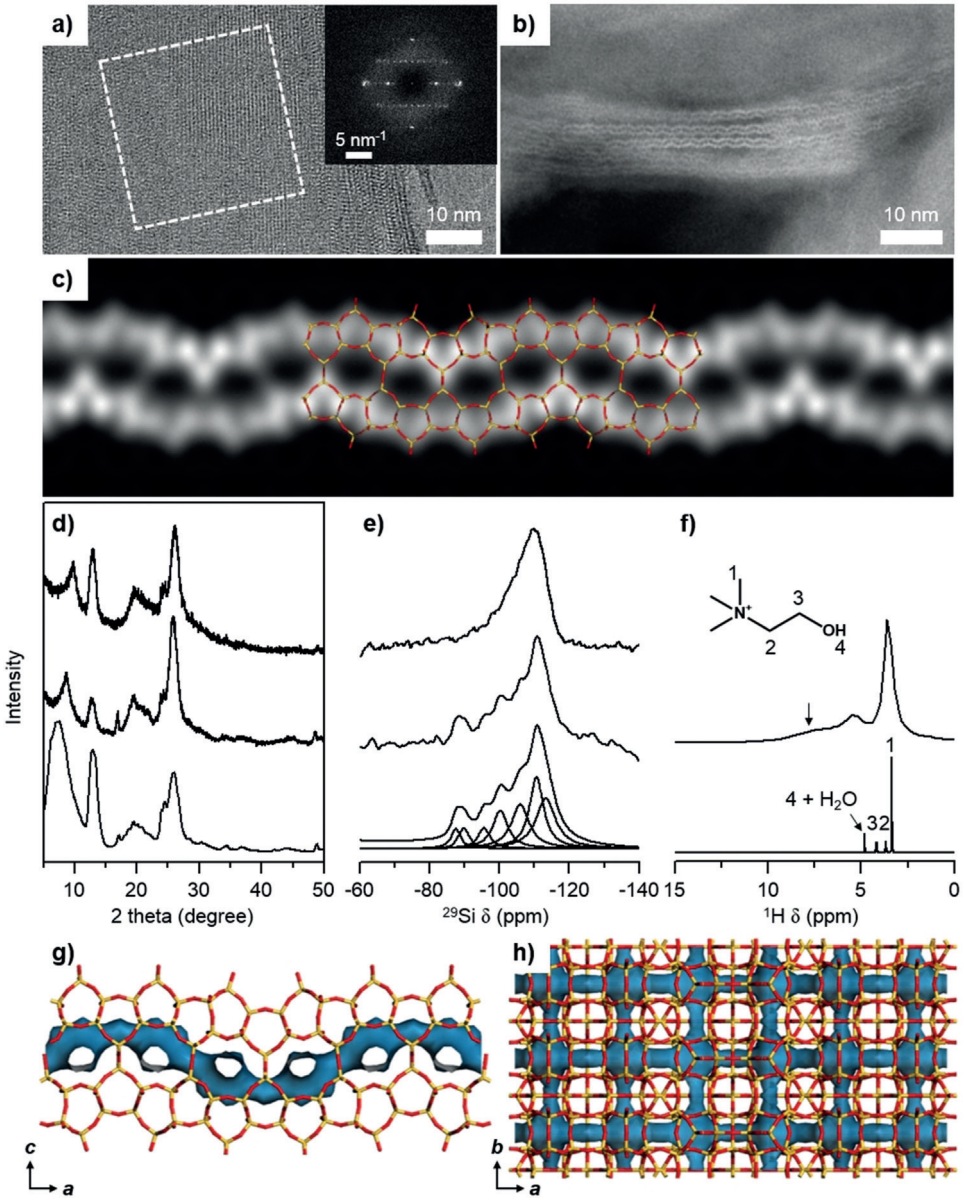

Figure 1. a) HRTEM image of as-made ChRbLi-PST-9 measured perpendicular to the nanosheet. Inset: its Fourier transform. b) ADF-STEM image of ChRbLi-PST-9 obtained along the *b*-axis after sectioning the nanosheet by ultramicrotome and c) projected potential map constructed based on the ADF-STEM image in plane group *pmg* showing the structure of PST-9 viewed along the *b*-axis. d) Simulated powder XRD pattern (bottom) from the structure model of a single layer of PST-9 with no extraframework cations and experimental (CuKα radiation, $\lambda = 1.541874$ Å) patterns of as-made (middle) and calcined (top) forms of ChRbLi-PST-9. e) Simulated (bottom) and experimental (middle) ^{29}Si MAS NMR spectra of as-made ChRbLi-PST-9. The experimental spectrum of (top) its calcined form is also given for comparison. f) ^{1}H NMR spectra of organic SDA, choline, showing the assignment of each resonance signal: ^{1}H NMR spectrum of (bottom) choline chloride in D_2O solution and ^{1}H MAS NMR spectrum of (top) ChRbLi-PST-9. The ^{1}H resonance assignable to Si–O^-···HOSi hydrogen bonds between defects is marked by an arrow. Structure of PST-9 viewed along the g) *b*- and h) *c*-axes. Yellow Si, red O.

ChRbLi-PST-9 shows signs of seven components ranging from approximately −88 to −113 ppm, where the three low-field components can be attributed to the Q^2 [$(SiO)_2Si(OH)_2$] and/or Q^3 [$(SiO)_3Si(OH)$] units.[8] We also found a weak, broad line around 8 ppm in its ^{1}H MAS NMR spectrum, assignable to the protons of the silanol (SiOH) groups involved in hydrogen bonding with neighboring Si-O^- groups[9] (Figure 1 e,f), which can be further evidenced by infrared spectroscopy (Figure S4).

Owing to the inherently broad nature of its powder X-ray diffraction (XRD) pattern (Figure 1 d), we used high-resolution transmission electron microscopy (HRTEM) and annular dark-field scanning TEM (ADF-STEM) to solve the structure of ChRbLi-PST-9. The Fourier transform (FT) of the HRTEM image taken perpendicular to the PST-9 nanosheet shows sharp diffraction spots (inset in Figure 1 a), indicating that PST-9 is ordered in at least two dimensions. The lattice parameters could be estimated from the FT of the image to be $a =$ 29.3 Å, $b = 7.5$ Å and $\gamma = 90°$. Neither channels nor cavities are visible from this projection. We therefore obtained ADF-STEM image of ChRbLi-PST-9 along the short 7.5 Å *b*-axis within the nanosheet (Figure 1 b), which shows that its structure consists of two sinusoidal layers with a pitch of ca. 30 Å, essentially identical to the 29.3 Å periodicity found from HRTEM. The projected potential map reconstructed from the ADF-STEM image reveals that the sinusoidal layer is constructed by edge-sharing 5-rings. A pair of the sinusoidal layers is connected to one another to form a double layer with 8-ring channels along the 7.5 Å *b*-axis (Figure 1 c). These findings suggest that PST-9 has a 2D layered structure with a lack of periodicity perpendicular to the nanosheet. The unit cell parameters of the PST-9 within the layer are $a = 29.3$ Å, $b = 7.5$ Å and $\gamma = 90°$. The four relatively sharp peaks in the powder XRD pattern in Figure 1 d can all be assigned as *hk*0 reflections; 410, 020, 800 and 040 for peaks at 16.9, 23.8, 24.3 and 48.6°, respectively. This further confirms the absence of the periodicity perpendicular to the layer.

According to our earlier findings,[10] a periodicity of 7.5 Å in zeolites likely corresponds to the presence of saw-tooth chains. This led us to expect that PST-9 would be built of saw-tooth chains aligned along the *b*-axis. Based on the projected potential map and the unit cell parameters, a structure model of the layer was built. An artificial *c*-axis perpendicular to the layers with a large *c*-parameter (100 Å) was used to keep the layers well separated. A space group (*Pmma*), which is compatible with the projection symmetry *pmg* of the ADF-STEM image, was determined by crystallographic image processing using CRISP (Figure 1 c).[11] We next performed the geometrical feasibility test on the structure model of the PST-9 layer using the unit cell parameters determined by powder XRD ($a = 29.21$ Å, $b = 7.46$ Å and $c = 100.00$ Å). The geometric refinement in space group *Pmma* gave the most suitable structure model with a geometrical residual (R_{dls}) of 0.0032. This is also supported by a reasonable match between the experimental and simulated powder XRD patterns (Figure 1 d); the weaker intensity in the low angle region of the experimental pattern is mainly due to the presence of extraframework cation species in ChRbLi-PST-9, which were not included in the XRD pattern simulation. The final atomic positions and selected bond lengths and angles of this 2D zeolite are given in Tables S2 and S3, respectively. The average T–O bond length (1.61 Å) and average O-T-O and T-O-T angles (109.5 and 153.6°, respectively) are in good agreement with those expected for zeolitic materials.

The framework structure of PST-9 contains an intralayer 2D pore system consisting of straight 8-ring (3.5×4.7 Å) channels along the *b*-axis intersected by sinusoidal 8-ring (3.7×4.8 Å) channels along the *a*-axis (Figure 1 g,h). No openings larger than 6-rings exist along the *c*-axis (perpendicular to the PST-9 sheet), partly explaining the low external surface area ($143\ m^2 g^{-1}$) of the proton form (H-PST-9) of ChRbLi-PST-9 determined by N_2 adsorption. Among the 13 topologically distinct T-atoms, only two (i.e., sites T3 and T7) of them terminate the external surface of the layers. We note here that not only the two unit cell dimensions of PST-9 and EU-12 are quite similar to each other,[1,6] but also both structures contain the saw-tooth chains that are combined to form 5-ring layers, which are ultimately connected to form 8-ring channels. The saw-tooth chains are only part of the 5-ring layers in the EU-12 structure. However, they are located between the two neighboring layers in the PST-9 structure, as well as within its 5-ring layers (Figure S6). Thus, PST-9 is structurally rather different from EU-12.

Calcination of as-made ChRbLi-PST-9 with the unit cell composition $|\text{choline}_{6.4}Rb_{1.1}Li_{0.5}(H_2O)_{17.3}|[Al_{6.1}Si_{67.9}O_{154}]$ at 550 °C to remove the occluded choline cations led to two observable changes in the powder XRD pattern (Figure 1 d); a shift of the first broad peak belonging to the (00*l*) family, from approximately 9 to 10° and a disappearance of the first sharp peak at 16.9°. However, although the structure projection images reconstructed from a through-focus series of HRTEM images show that HRbLi-PST-9 preserves its layered structure, some wavy PST-9 layers were changed into flat layers with a reduction in the interlayer distance (Figure S7). The reason why no topologically related 3D zeolite structures were obtained by the condensation of individual PST-9 layers may be the vertical mismatch between opposing SiOH groups on adjacent layers owing to considerable disorder in the layer packing. Thus, the discovery of PST-9, together with MCM-56, raises the question of whether the concept of novel zeolite structures can be extended to 2D zeolitic materials.

Infrared spectroscopy with adsorbed small ammonia and larger pyridine shows that the concentration of Brønsted acid sites in H-PST-9 determined using the former adsorbate is about 15 times higher than the value obtained using the latter one (Table S4). Therefore, most of the framework Al atoms in this 2D zeolite appear to be buried in the intralayer 8-ring channels, like the case of MCM-22(P).[2] As shown in Figure 2 a, on the other hand, PST-9, obtained after 2 days of heating at 150 °C in the choline-Rb^+-Na^+ mixed-SDA system, is completely transformed to EU-12 when heated for additional 5 days in the crystallization medium. The ^{13}C MAS NMR, infrared and Raman spectroscopy results in Figure 2 and Figure S8 clearly show that choline remains intact within the void space of a series of solid products recovered not only during the crystallization of ChRbNa-PST-9, but also during its phase transformation to ChRbNa-EU-12. This asymmetric quaternary ammonium cation is known to exist primarily as a *gauche* conformer in the solid, liquid and gas phases, because of the stabilization by non-specific, electrostatic interactions between the electronegative oxygen atom of the OH group and the positive charge distributed over its head $[(CH_3)_3N^+CH_2]$ group.[12]

However, as corroborated by the relative intensities of the two Raman bands around 710 and 760 cm^{-1}, shown in Figure 2 b, from the symmetric C–N stretching mode (ν_s(C–N)) of *gauche* and *trans* choline conformers, respectively,[12a] the *gauche*/*trans* conformer ratio in solid products separated during PST-9/EU-12 synthesis at 150 °C rapidly decreases with increasing crystallization time to 2 days, that is, until PST-9 fully crystallizes. This can be rationalized by taking into account the narrow 8-ring channels of PST-9 within which the *trans* conformer, thinner than the *gauche* conformer, may be easily encapsulated. It is also remarkable that repeated K^+ ion exchange of ChRbNa-PST-9 led to a disappearance of the ν_s(C–N) band around 710 cm^{-1} (Figure S9). When combined with the TGA/DTA results in Figure S3, therefore, approximately one third of choline ions in this 2D zeolite seem to be present as the *gauche* conformer at exchangeable sites, that is, in the interlayer region. The *gauche*/*trans* ratio of occluded choline further decreases during the phase transformation of PST-9 to EU-12, although the extent of its decrease is small compared with that found during PST-9 crystallization (Figure 1 d). As a result, choline cations exist predominantly as the *trans* conformer in ChRbNa-EU-12, again due to their location within the 8-ring channels of EU-12 that are even narrower than those in PST-9.[1]

Another interesting finding from Figure 2 is that while the intensity of the methyl carbon resonance at 53.7 ppm in the ^{13}C MAS NMR spectra of solid products isolated during PST-9/EU-12 synthesis decreases with increasing crystallization time, thus being barely observable in the spectrum of ChRbNa-EU-12, the opposite holds for the resonance at 55.4 ppm due to the methylene carbon bonded to the oxygen

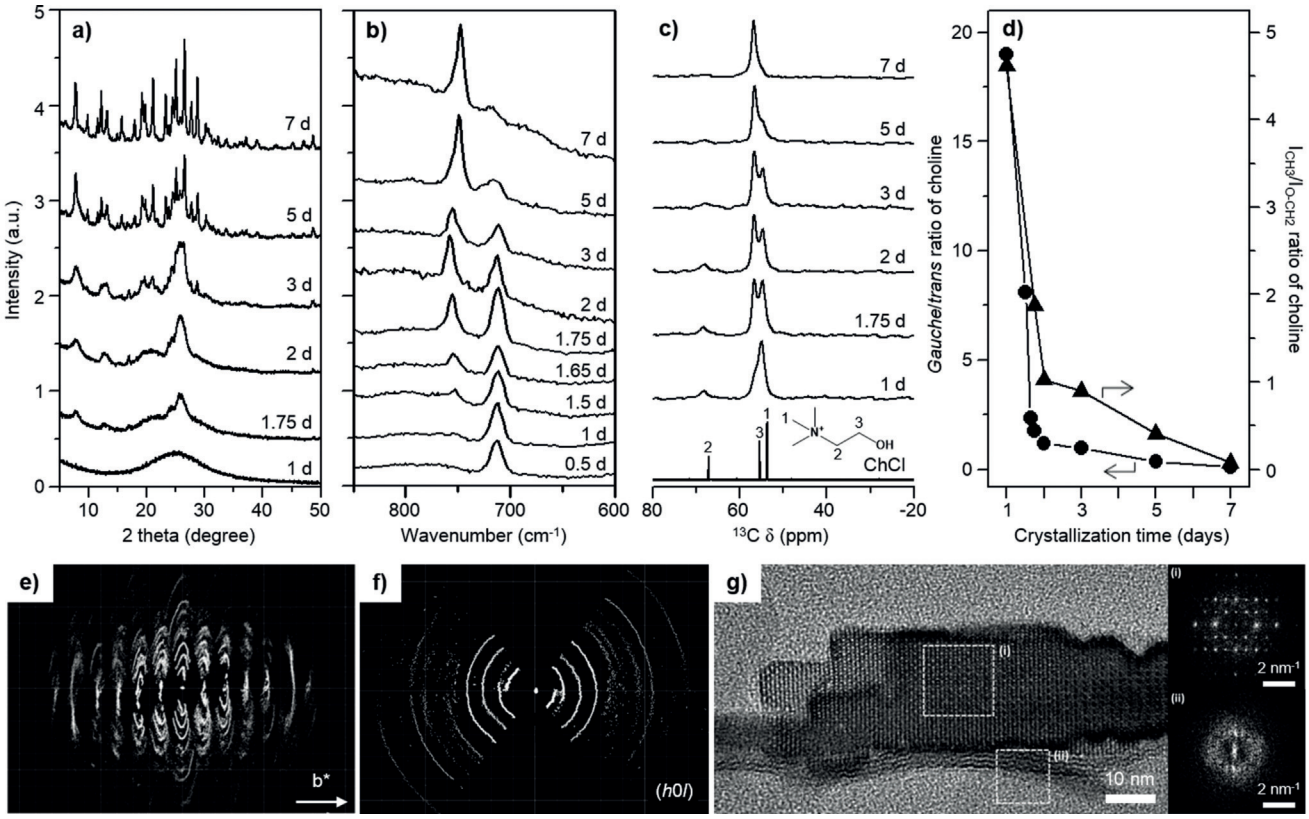

Figure 2. a) Powder XRD patterns, b) Raman, and c) ^{13}C MAS NMR spectra of a series of solid products separated as a function of time during PST-9/EU-12 synthesis at 150 °C in the choline-Rb^+-Na^+ mixed-SDA system. Note that the solid products isolated after 2 and 7 days of heating are as-made ChRbNa-PST-9 and ChRbNa-EU-12, respectively. d) *Gauche*/*trans* ratio (●) of choline cations in solid products isolated at different times calculated from the intensities of two Raman bands around 710 and 760 cm^{-1} seen in (b) and intensity ratio (▲) of ^{13}C MAS NMR resonances arising from methyl and methylene carbon atoms (bonded to the oxygen atoms), appearing at 53.7 and 55.4 ppm in the spectra in (c). e) 3D reciprocal lattice of the solid product isolated after 3 days reconstructed from the cRED data and f) 2D (*h*0*l*) slice cut from its reconstructed 3D reciprocal lattice. g) Structure projection image of the solid product recovered after 5 days. The wavy PST-9 layers can be found on the surface of EU-12 crystals, which can be further supported by the Fourier transforms in the two insets.

in choline. Apparently, the chemical environment of this organic SDA must become spatially more restricted during the transformation of 2D PST-9 to 3D EU-12, since the methylene group in choline is much thinner than its trimethyl group. We also note that there are no noticeable changes in the organic content during this transformation, as well as in the yield (56 ± 2 wt %) of solid products (Table S5). Considering all these results, therefore, the phase transformation cannot be explained by the traditional dissolution/recrystallization process.

To elucidate the phase transformation mechanism of PST-9 in the choline-Rb^+-Na^+ mixed-SDA system, we characterized a series of solid products separated after heating at 150 °C for different times using TEM and electron diffraction. As shown in Figure S10, the selected-area electron diffraction (SAED) pattern of the solid product (i.e., as-made ChRbNa-PST-9) obtained after 2 days of heating, although showing no preferred orientation, appears as concentric rings whose *d*-values are consistent with the PST-9 structure. After 3 days, the product was not randomly bended nanosheets, but stretched out in one dimension. Electron diffraction shows that the 7.5 Å periodicity is well defined (Figure S10c), although diffuse scattering appears as streaks running perpendicular to the *b*-axis. From the TEM image it seems that the original PST-9 layer is folding around its extending *b*-axis during the transformation process. It should be noted that the final product ChRbNa-EU-12, which crystallized as very thin and long plates after 7 days (Figures S10 and S11), also has its periodicity of 7.5 Å along the longest dimension of its crystals. Given that the *b*-axis of ChRbNa-EU-12, the direction of the layers of edge-sharing 5-rings, runs along the shortest dimension of the crystals, the transformation from PST-9 to EU-12 cannot be a simple condensation of the PST-9 layers but rather a folding around the axis with 7.5 Å periodicity.

Further evidence for this hypothesis can be obtained from continuous rotation electron diffraction (cRED) studies. The 3D reciprocal lattice reconstructed from the cRED data of the solid product obtained after 3 days shows a well-defined periodicity along the 7.5 Å axis and concentric arcs around the same axis (Figure 2e). 2D sections cut from the reconstructed 3D reciprocal lattice exhibit arcs in the plane perpendicular to the *b*-axis (Figure 2f). It is thus clear that the crystal structure is extending with a periodicity of 7.5 Å in one dimension, whereas the nanosheet is bending or folding around the same axis. The contrast in Figure S10c also reveals that while the nanosheet is folding at the edges, features are

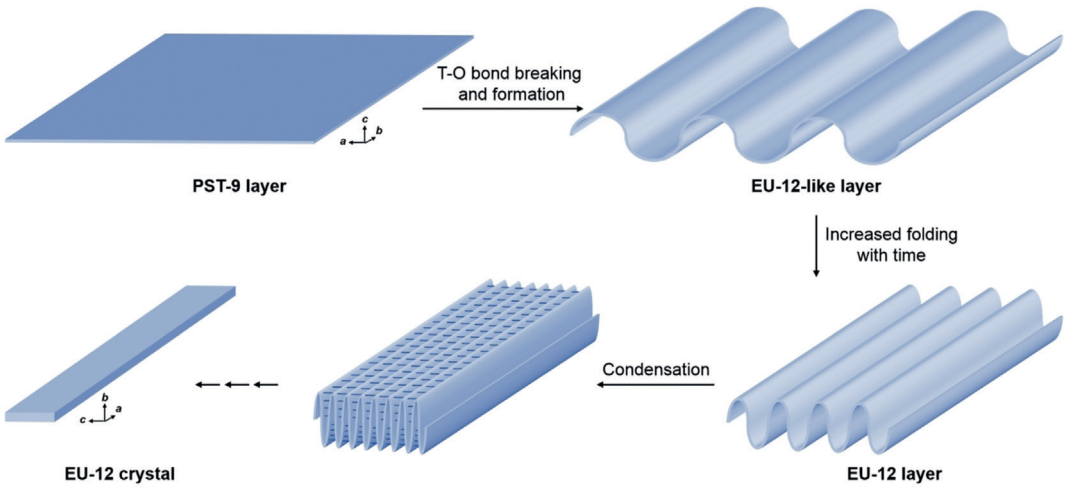

Figure 3. Schematic illustration of a possible phase transformation pathway of PST-9 into EU-12 in the choline-Rb^+-Na^+ mixed-SDA system.

extending along the 7.5 Å axis in the center of the forming crystal. On the other hand, a structure projection image of the intermediate product isolated after 5 days, which has not yet been fully transformed to EU-12, shows the wavy PST-9 layers located on the surface of the EU-12 crystal (Figure 2g). We note that both materials are imaged along their shortest crystallographic axis. This indicates that the two materials align their saw-tooth chains during the transformation process.

Figure 3 shows a possible transformation pathway from PST-9 to EU-12 based on the characterization results presented thus far. Considering the structural differences between PST-9 and EU-12 layers, the transformation cannot proceed without the breaking of some T–O bonds in the single PST-9 layer followed by the formation of new T–O bonds, leading to an EU-12 structure. This looks reasonable, because we could not find any experimental evidence supporting the existence of EU-12 layers from all of our PST-9/EU-12 syntheses. One possible formation pathway of the EU-12-like layer through the breaking and formation of particular T–O bonds in the PST-9 layer can be found in Figure S12. A combination of elemental and thermal analysis reveals that the onset of transformation in the choline-Rb^+-Na^+ mixed-SDA system causes a sharp decrease in Rb^+/Al ratio, together with an increase in choline/Al ratio, in the solid product (Figure S13). This suggests that choline plays a much more important role in the EU-12 layer formation than Rb^+. Also, since there are no noticeable changes in Na^+/Al ratio during the phase transformation, the role of Na^+ appears to be negligible. The other requirement for the phase transformation process is that the EU-12-like layer should be flexible enough to be folded when continuously formed. This could be enabled by a selective T–O bond breaking perpendicular to the extended 7.5 Å axis. After folding of the nanosheet the remaining unconnected T–O bonds will be connected in order to create the final 3D EU-12 structure.

To date, there is one case where ion exchange of interlayer Na^+ ions in the layered silicate kanemite with long-chain surfactant cations directs the formation of mesoporous materials FSM-16 with a hexagonal array of uniform channels, because the kanemite layers can wind around the exchanged surfactant species.[13] Therefore, the folding growth mechanism proposed herein is substantially different than any known mechanism of phase transformation and crystal growth of ordered nanoporous materials.[14] Finally, it is worth noting that the replacement of choline with an equimolar amount of bis(2-hydroxyethyl)dimethylammonium ions, which contain one more ethanol group than the choline organic SDA, in the choline-Rb^+-Na^+ mixed-SDA system directly yielded EU-12, without having PST-9 as an intermediate (Figures S11 and S14). This indicates that zeolite crystal growth mechanism can differ according to the type of organic SDAs used, which deserves further study.

In summary, we have synthesized a novel 2D zeolite, PST-9, whose intralayer region contains straight 8-ring (3.5 × 4.7 Å) channels along the *b*-axis intersected by sinusoidal 8-ring (3.7 × 4.8 Å) channels along the *a*-axis, using choline as an organic SDA via the multiple inorganic cation approach. Both its layered nature and intralayer microporosity remain almost intact, even after calcination at 550 °C to remove the occluded organic SDA, which is mainly a result of mismatch between the terminal SiOH groups on adjacent PST-9 layers. PST-9 was found to undergo an in situ transformation to 3D zeolite EU-12 in the choline-Rb^+-Na^+ mixed-SDA system through the single-layer folding mechanism. Our study provides new insights into the growth mechanisms of zeolites and related crystalline materials, as well as into their phase transformation mechanisms.

Acknowledgements

We acknowledge financial support from National Creative Research Initiative Program (2012R1A3A-2048833) through the National Research Foundation of Korea, the National Research Council of Science & Technology (CRC-14-1-KRICT) grant by the Korea government (MSIP), the Swedish Research Council (2017–04321), and the Knut and Alice Wallenberg Foundation (KAW) through the project grant 3DEM-NATUR (2012.0112). T.W. acknowledges an interna-

tional postdoc grant from the Swedish Research Council (2014-06948).

Conflict of interest

The authors declare no conflict of interest.

Keywords: crystal growth · folding mechanism · layered zeolites · phase transformation · structure elucidation

How to cite: *Angew. Chem. Int. Ed.* **2019**, *58*, 10230–10235
Angew. Chem. **2019**, *131*, 10336–10341

[1] C. Baerlocher, L. B. McCusker, Database of Zeolite Structures: http://www.iza-structure.org/database/ (accessed March 20, 2019).
[2] W. J. Roth, P. Nachtigall, R. E. Morris, J. Čejka, *Chem. Rev.* **2014**, *114*, 4807–4837.
[3] a) M. K. Rubin, P. Chu, US Pat 4954325, **1990**; b) M. E. Leonowicz, J. A. Lawton, S. L. Lawton, M. K. Rubin, *Science* **1994**, *264*, 1910–1913.
[4] M. Choi, K. Na, J. Kim, Y. Sakamoto, O. Terasaki, R. Ryoo, *Nature* **2009**, *461*, 246–249.
[5] a) A. S. Fung, S. L. Lawton, W. J. Roth, US Pat 5362697, **1994**; b) J. E. Schmidt, D. Xie, M. E. Davis, *Chem. Sci.* **2015**, *6*, 5955–5963; c) B. Marler, M. Müller, H. Gies, *Dalton Trans.* **2016**, *45*, 10155–10164.
[6] J. Bae, J. Cho, J. H. Lee, S. M. Seo, S. B. Hong, *Angew. Chem. Int. Ed.* **2016**, *55*, 7369–7373; *Angew. Chem.* **2016**, *128*, 7495–7499.
[7] J. Shin, D. Jo, S. B. Hong, *Acc. Chem. Res.* **2019**, *52*, 1419–1427.
[8] G. Engelhardt, D. Michel in *High-Resolution Solid-State NMR of Silicates and Zeolites*, Wiley, Chichester, **1987**.
[9] H. Koller, R. F. Lobo, S. L. Burkett, M. E. Davis, *J. Phys. Chem.* **1995**, *99*, 12588–12596.
[10] P. Guo, N. Yan, L. Wang, X. Zou, *Cryst. Growth Des.* **2017**, *17*, 6821–6835.
[11] T. Willhammar, Y. Yun, X. Zou, *Adv. Funct. Mater.* **2014**, *24*, 182–199.
[12] a) H. Akutsu, *Biochemistry* **1981**, *20*, 7359–7366; b) J. Bae, S. B. Hong, *Chem. Sci.* **2018**, *9*, 7787–7796.
[13] S. Inagaki, Y. Fukusima, K. Kuroda, *J. Chem. Soc. Chem. Commun.* **1993**, 680–682.
[14] C. S. Cundy, P. A. Cox, *Microporous Mesoporous Mater.* **2005**, *82*, 1–78.

Manuscript received: April 18, 2019
Accepted manuscript online: May 22, 2019
Version of record online: June 24, 2019

